International Journal of Computers and Applications

ISSN: 1206-212X (Print) 1925-7074 (Online) Journal homepage: http://www.tandfonline.com/loi/tjca20

3D reconstruction of skeletal mesh models and human foot biomodel generation using semantic parametric-based deformation

Alexander Agathos & Philip Azariadis

To cite this article: Alexander Agathos & Philip Azariadis (2018): 3D reconstruction of skeletal mesh models and human foot biomodel generation using semantic parametric-based deformation, International Journal of Computers and Applications, DOI: 10.1080/1206212X.2018.1443316

To link to this article: https://doi.org/10.1080/1206212X.2018.1443316

Published online: 20 Mar 2018.

INTERNATIONAL JOURNAL OF COMPUTERS AND APPLICATIONS, 2018
https://doi.org/10.1080/1206212X.2018.1443316

Taylor & Francis
Taylor & Francis Group

3D reconstruction of skeletal mesh models and human foot biomodel generation using semantic parametric-based deformation

Alexander Agathos and Philip Azariadis

Department of Product & Systems Design Engineering, University of the Aegean, Ermoupolis, Greece

ABSTRACT

This paper introduces two methodologies for the reconstruction of skeletal mesh models and for the generation of parametric bone models of the human foot. First, a new Parametric-Based Deformation methodology is presented, which deforms a template 3D mesh according to user-defined semantic parameters in order to derive a new bone model. The proposed method allows the parameterization of dense and detailed 3D meshes of human foot bones. An extensive evaluation is performed to examine the accuracy, quality, and performance of the proposed method with human and animal bones, and versus existing statistical-based methods in the literature. Also, a novel methodology is proposed for the generation of parametric bone models of the human foot using non-calibrated biplanar X-rays. The proposed method has been applied for the production of detail 3D foot biomodels from an initial template biomodel and has been evaluated using human and animal bones.

ARTICLE HISTORY
Received 10 February 2018
Accepted 18 February 2018

KEYWORDS
3D bone reconstruction; parametric-based deformation; skeletal models; human foot biomodel; semantic parameters

1. Introduction

The process of automatic generation of a 3D model which belongs in a specific category like a human body, face or bone, with specific semantic parameters is an important topic in CAD/Computer Graphics and medical image analysis. There is a plethora of applications involved in this process, like for example crowd simulation, animation and garment design based on specific body-type and height. Concerning bones, this process is crucial because it reduces the time a bone is reconstructed compared to density-segmentation methods [1] which is vital for *in vivo* situations like quick diagnosis from the doctor and fast/accurate surgery preparation [2,3]. Also, by this way the patient is not exposed to hazardous CT scan radiation, while the need for undergoing the tedious process of MRI scan is minimized. Parametric bone reconstruction is important in applications which employ bioengineering analysis with the use of Finite Element Method (FEM).

The area of works parameterizing the human body is based on the concept of deforming a template 3D mesh model or a 3D range scan according to various semantic anthropometric parameters (attributes), providing a novel individual human body. Many works utilize principal component analysis (PCA) to statistically define the space of deformations of a given 3D model. In [4], a template 3D human model is deformed to match the 3D scan of a human subject using human weight and height as semantic parameters. In [5], a template model is deformed to match the range scan of the human body using a semi-automatic non-rigid registration algorithm. This method is able to describe both human pose and body shape providing realistic character animations. In [6], a template body model is chosen from a variety of template models using PCA that best fits (closest PCA parameters) to a scanned human body. In [7], the shape of scanned people is determined in relation to given anthropometric measurements where a template model is deformed to match human range scans. Using PCA the template model is correlated with anthropometric semantic parameters like height and weight. The same model is adopted in [8], though this time a regression analysis is used to correlate the feature vector derived from PCA to the anthropometric parameters.

In [9], a silhouette extraction method and a feature-based reconstruction approach is proposed to reconstruct a human body from two orthogonal images. The proposed approach identifies and establishes a connection between feature points of the silhouettes extracted on the images and the predefined silhouettes of a template mannequin. In [10], a new human model is derived

CONTACT Philip Azariadis azar@aegean.gr

by minimizing a function between a specific model and semantic parameters using linear interpolation over the entire population of a mannequin database. In [11], the work of [10] is used up to the level of acquiring the feature based model. Then PCA is applied to correlate these features with anthropometric semantic parameters.

In the specific area of parameterization of human bones, a similar concept is usually followed. A template bone, which is generated either geometrically or statistically, is deformed to match a target bone using statistic or geometric parameters.

In [12], active set models [13] are used to reconstruct a statistical model of the femur bone. Although the statistical model constructed by active set models is quite flexible because it deforms according to a set of weights, the correlation of these weights with the user-defined parameters is not straightforward. In [3], a method to reconstruct the proximal femur bone from two or more calibrated X-rays using a statistical method and a template bone is proposed. The template bone represents the mean shape from a sample database. A similar approach is followed in [2], where a statistical model of the distal femur is derived through PCA. This method requires a clear and without overlaps fluoroscopic projection of the bone on the X-ray, while the reconstruction results have an orientation dependency. In [5], a parametric model is used to reconstruct the proximal epiphysis of the femur. Using a database of sample femur bones and linear regression, a novel femur bone is reconstructed using the algorithm presented in [14].

Template parametric models are also used for the reconstruction of spline, see e.g. works [15,16]. In [16], spine samples are used to correlate eight landmarks with 21 3D data points on the vertebral body using linear regression. A surface reconstruction algorithm is used to reconstruct the vertebral shape from these 3D data points. The work of [15] improves [16] by considering also a parametric longitudinal inference of the spine.

Despite the large number of dedicated works only a few address the parameterization of the human foot. In [17], the outer shape of the human foot is parameterized using a population of 40 men and tested on 25 men. The parameters used are the foot height, width, length, and curvature. In [18], two methods to generate an individual 3D foot shape from 2D information are proposed. The first method utilizes the 2D outline and height, while the second method utilizes the 2D outline and the 2D profile of the foot. These methods provide only the outer surface of the foot and they are not suitable for applications relying on Finite Element Analysis (FEA) which require the development of a detailed 3D foot biomodel.

In [19], a method is proposed to simulate the deformation of the foot using the Boundary Elements Method (BEM). A human foot is scanned using reflective markers which are tracked during gait by a set of eight cameras. Utilizing the marker locations, the skin surface is deformed to match certain phases of the walking cycle by applying BEM. Then the foot is manually aligned with a simplified footwear model and a stress–strain problem is solved to identify areas of peak pressures. The proposed approach is not parameterized and, therefore, the entire procedure has to be repeated for every different human foot.

A recent work dealing with the parametric modification of skeletal models is proposed in [20]. The generation of bone shapes is achieved by a methodology which requires sample bones of the same class to construct a fairly robust template model. This template model is later modified according to the introduced geometric parameters. The overall modeling process is divided into three stages: template construction (production of a template bone model), regression (generation of best fitting deformation model), and prediction (generation of the new bone instance based on the given parameters). The regression stage of this methodology is based on an iterative process where a steepest descent algorithm and a t-FFD deformation are utilized. However, there is no guarantee that the process will converge, and the final error metric will be minimized.

In this paper, we will present two novel methodologies. Specifically, the original work reported in [20] is revisited and an improved algorithm is proposed, while the second methodology presents a new algorithm for automatic generation of foot bones using non-calibrated biplanar X-rays. With the two methodologies proposed in this paper one can develop a parametric biomodel of the foot that can be used for bioengineering analysis based on the FEM. Preliminary results of this work were presented in [21], where the basic idea of parametric bone reconstruction and some illustrations of a biomodel production experiment were briefly presented. The present paper, describes in-detail both methodologies along with a thorough evaluation using experimental and real-world data. To all our knowledge, no previous work addresses the development of a parametric foot biomodel.

The first methodology presented in this paper describes a new pipeline for the parametric modification of 3D skeletal models and replaces the regression stage of [20] with a new robust procedure. With the modified method, we are able to handle detailed models with thousands of triangle elements. The proposed method has been evaluated with human and animal bones and it has been compared against the original approach and statistical methods relying on PCA, like [4,11], providing superior results in all cases. The second methodology, utilizes the proposed parametric method to reconstruct foot bones

using a semi-automatic procedure and a biplanar X-ray. With this method, custom foot biomodels can be produced from a template 3D biomodel. Contrary to previous approaches, like [2,3,5,15,22] there is no need for special equipment or calibrated X-rays. This method has been evaluated using human bone samples taken from biplanar X-rays and CT-scans, and animal bones acquired through 3D scanning.

The first methodology is presented in Section 2, while the second is presented in Section 3. Both methodologies are evaluated in Sections 4 and 5, respectively. Section 6, provides conclusions and ideas for future research.

2. Parametric-based deformation methodology of skeletal models

The goal of the current parameterization methodology is to utilize a given prototype 3D mesh P and deform it according to given parameters $(p_1^M, p_2^M, \ldots, p_k^M)$ to a new 3D mesh M. The parameters vector characterizes the set of 3D meshes that can be generated from P. For example, let's consider the 3D mesh of the talus bone of the human foot (Figure 1). One possible parameterization of this shape can involve its length, width, and height. Different values of these parameters will produce different instances of the talus bone. In practice, one should select the type and number of semantic parameters with respect to the corresponding application.

The proposed methodology is divided into three basic stages which are illustrated in Figure 1, with the talus bone as an example. A mesh simplification [23] that preserves topology is applied to P acquiring mesh P_c, which will be called as control mesh from now on. In the first stage, a mapping between the prototype mesh P with the control mesh P_c is established. At the second stage, the control mesh P_c is modified using a linear transformation with parameters $(p_1^M, p_2^M, \ldots, p_k^M)$ deriving the control mesh P'_c. At the third stage, the modified control mesh P'_c is used to deform mesh P into M. The last deformation utilizes the mapping established in the first stage. The new mesh M conforms approximately to the user input parameters $(p_1^M, p_2^M, \ldots, p_k^M)$.

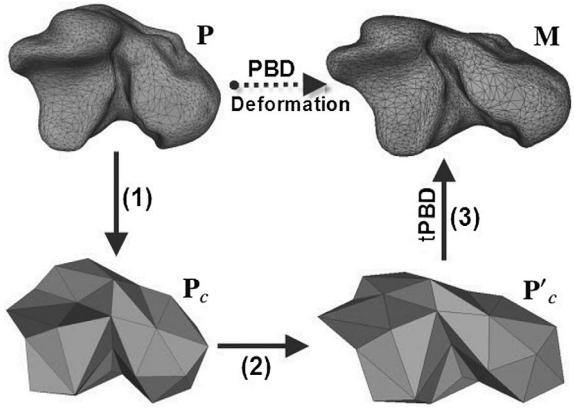

Figure 1. The basic stages of the proposed methodology: (1) Generation of $\mathbf{P}_c$ and establishment of relationship between **P** and $\mathbf{P}_c$. (2) Modification of the control mesh $\mathbf{P}_c$ to $\mathbf{P}'_c$ using the input parameters. (3) Generation of the new deformed shape **M**.

In matrix notation, the linear transformation of Stage 2 can be expressed as:

$$\mathbf{P}'_c = \mathbf{A}\left(p_1^M, p_2^M, \ldots, p_k^M\right)^{\mathrm{T}} \tag{1}$$

where P'_c stands for the vertices of the control mesh. The transformation matrix A is defined on the space of the simplified model to work with much fewer degrees of freedom and to increase the approximation precision to the given parameters $(p_1^M, p_2^M, \ldots, p_k^M)$.

In this paper, the overall process which deforms the prototype mesh P to M will be denoted as **PBD** and stands for *Parametric-Based Deformation*. Stage 3 is denoted in function notation as **tPBD**, which stands for *triangular Parametric-Based Deformation*, receiving as argument the modified control mesh P'_c and producing as output the deformed model. So, in function notation, Stage 3 is expressed as:

$$t\mathbf{PBD}\left(\mathbf{P}'_c\right) = \mathbf{M} \tag{2}$$

In the sequel, stage 1 will be briefly described as we focus mainly on the second stage of the proposed methodology (i.e. the calculation of transformation matrix A) since this is the most crucial operation in the deformation process.

2.1. Stage 1: mapping of the prototype mesh P to the control mesh P_c

To each of the triangles P_c^i of the control mesh P_c, a local coordinate system Ξ_i is assigned according to the t-FFD methodology [24], where each point q of P has coordinates (u_i, v_i, w_i) in Ξ_i. A weight k_i is defined which denotes the effect of triangle P_c^i to the point q of P. Thus, each point q of P is related to each triangle P_c^i of P_c with the quartet (u_i, v_i, w_i, k_i).

2.2. Stage 2: deformation of the control mesh P_c to the control mesh $\mathbf{P}'_c$

In order to establish the linear transformation of Equation (1), a set of sample meshes with known parameters is required. Let's denote a member of the sample set as $S \neq P$. Figure 2 depict the detailed steps to acquire matrix A. Steps 1.1 to 1.4 are applied to all samples S.

The process of deforming the control mesh is the inverse of deforming the prototype mesh thus this deformation

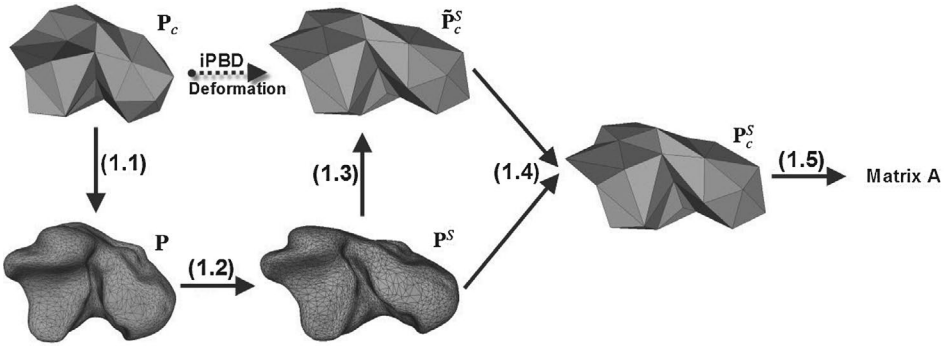

Figure 2. Calculation of matrix **A**: (1.1) Establishment of a mapping between $\mathbf{P}_c$ and **P**. (1.2) Modification of the mesh **P** to $\mathbf{P}^S$ using affine transformation. (1.3) Generation of the control mesh $\tilde{\mathbf{P}}_c^S$. (1.4) Least-squares minimization to compute control mesh $\mathbf{P}_c^S$. (1.5) Computation of matrix **A** using pseudo-inverse.

is called *inverse Parametric-Based Deformation* and is denoted as **iPBD**. Steps 1.1 and 1.3 are implemented using the same t-FFD concept described in Section 2.1.

In order to improve the robustness of the proposed algorithm, compared to the original version reported in [20], we have introduced Step 1.2 which utilizes an affine transformation procedure to register the prototype mesh P with the current sample mesh S. The registration procedure is based on [25]; a brief description of the underlying algorithm that has been implemented in this work is given in the following.

The vertices of the prototype mesh P are registered using an affine transformation $TP + b$ to the vertices of S, where, $T \in \mathbb{R}^{3\times3}$, P a vertex of P and $b \in \mathbb{R}^{3\times1}$. The transformed prototype mesh P is written as $TP + b$. It is assumed that both meshes P and S are roughly aligned like in Figure 3(a). Applying the affine transformation, mesh P (red bone) is affinely deformed and registered to mesh S (green bone), as it is shown in Figure 3(b).

The procedure of the affine registration consists of two parts: a global affine registration where all points of P are deformed and registered to S with the same affine matrix $T \in \mathbb{R}^{3\times3}$, and a local affine registration where each point of P is deformed and registered to S with its own affine matrix. At the first part, global geometric characteristics, like the size and shape, are taken into account, and at the second part local geometric characteristics are registered.

Using the mapping computed at Step 1.1 and the modified prototype P^S, the control mesh P_c is modified to the new control mesh $\tilde{\mathrm{P}}_c^S$. This new control mesh is derived by applying the t-FFD operator to the mesh P_c using the precomputed mapping parameters at Step 1.1. Then, a least-squares optimization problem is solved to compute the control mesh P_c^S:

$$\mathbf{P}_c^S = \underset{\hat{\mathbf{P}}_c^S}{\operatorname{argmin}} \left|\left|\mathbf{tPBD}\left(\hat{\mathbf{P}}_c^S\right) - \mathbf{P}^S\right|\right|^2 \tag{3}$$

where, $\hat{\mathrm{P}}_c^S$ is the vector of the unknown points of the control model P_c^S. For the solution of (3) the control model $\tilde{\mathrm{P}}_c^S$ is used as an initial (guess) solution. The optimization problem is solved using the Levenberg–Marquardt algorithm [26].

Assuming that n sample meshes $\mathrm{S}_i, i = 1, \ldots, n$ are available and the parameter space is k-dimensional, a linear correlation between the control models $\mathrm{P}_c^{S_i}$ and their respected user-defined parametric values $\left(p_1^{S_i}, p_2^{S_i}, \ldots, p_k^{S_i}\right)$ $i = 1, \ldots, n$, is assumed, according to the following equation:

$$\left[\begin{array}{cccc} \mathbf{P}_c^{S_1} & \mathbf{P}_c^{S_2} & \ldots & \mathbf{P}_c^{S_n} \end{array}\right] = \mathbf{A}\left[\begin{array}{cccc} 1 & 1 & \ldots & 1 \\ p_1^{S_1} & p_1^{S_2} & \ldots & p_1^{S_n} \\ \vdots & \vdots & \ddots & \vdots \\ p_k^{S_1} & p_k^{S_2} & \ldots & p_k^{S_n} \end{array}\right] \tag{4}$$

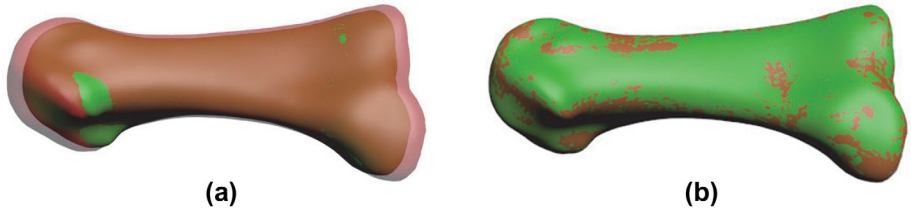

Figure 3. Two 3D bone meshes of the 1st metatarsal of the human: (a) roughly aligned and (b) registered using affine registration.

Matrix A is computed with the method of the pseudo-inverse [27]. Then the required control mesh P'_c is calculated using Equation (1).

3. Semi-automatic generation of human foot bones from bi-planar X-rays

In foot biomechanics, 3D biomodels are used for material sensitivity studies [28,29] and for investigating the effects of insole geometry on plantar pressure distribution [30,31]. A new methodology to produce a parametric foot biomodel is proposed, where the basic input is a set of biplanar foot X-rays. Contrary to other approaches that require special equipment and calibrated X-rays (e.g. [2,3,15,22]), the only known information on the X-rays used in this work is the dpi resolution, which provides an accurate measurement of the real width and height image dimensions.

The proposed methodology for deriving parametric human foot biomodels utilizes the parametric reconstruction method described in Section 2 to produce the necessary parametric bone models of the foot. The only user input required are the contours provided by an experienced user like a radiologist. For example, Figure 4 shows the contour lines of the metatarsal bones in the top view (DP) and side view (Oblique). The proposed method is described in Algorithm A.

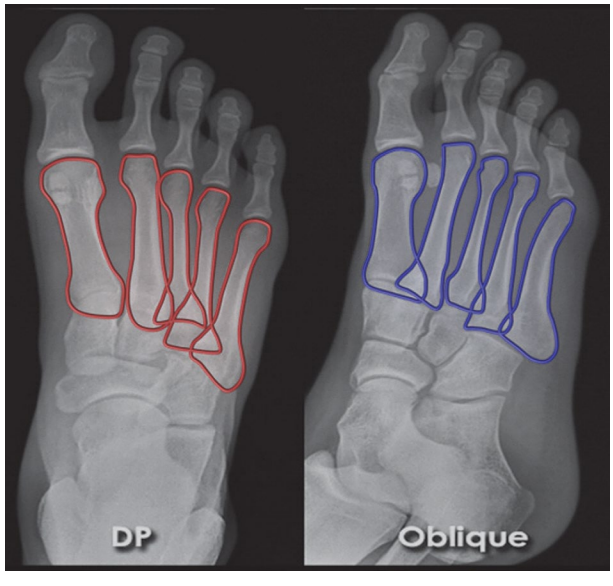

Figure 4. A biplanar X-ray of the lower human foot where the contour lines of the metatarsal bones have been highlighted. DP view: red-line contours. Oblique view: blue-line contours.

Algorithm A: Semantic bone parameterization

Input: Biplanar X-ray, bone contours in both views, prototype and sample bones
Output: Parametric bone model
Begin
Step A.1: Calibration of the prototype bone on the two views of the X-ray. The process provides a rigid transformation (R_i, t_i), $i = \{left, right\}$.
Step A.2: Application of (R_i, t_i) on all sample bones and calculation of the silhouette contour S_i, $i = \{left, right\}$, from the cut of the bone with the plane $z = 0$.
Step A.3: Calculate (automatically) the semantic parameters on each contour S_i.
Step A.4: Derive the corresponding parametric bone model.
Step A.5: Produce the custom bone by modifying the semantic parameters of the parametric bone model according to the new X-ray measurements.
End

Analytically, in Step A.1, we calibrate the prototype bone on the two views of the X-ray to fit as best as possible to the given contour curves. A rigid transformation (R_i, t_i), $i = \{left, right\}$ is calculated using [25,32]. The rays of the X-ray scanner intersecting the silhouette contours of the object (red, blue curves in our case) are rotated and translated by a least squares algorithm so as to be optimally tangential to the 3D object (see Figure 5(a)). The results of this step are depicted in Figure 5(b). In Step A.2, we align all sample bones with the silhouette contour on each view by applying the rigid transformations of Step A.1. Next, we find the silhouette contour $S_i, i = \{\text{left, right}\}$, from the cut of the bone with the plane $z = 0$. In Step A.3, using the silhouette contour S_i, we extract automatically the semantic parameters needed for the calculation of the parametric model presented in Section 2. In Step A.4, the parametric model is calculated from the semantic parameters and then in Step A.5 a custom bone model is created by modifying the semantic parameters according to the measurements of the new X-ray.

4. Experimental evaluation of the proposed parametric bone deformation method and comparison with previous approaches

A comparison against the previous method proposed by Lee and Joneja [20] and against statistical-based methods, like [4,11], that utilize PCA has been conducted to examine the benefits of the new parametric bone deformation approach. The quality of the derived meshes has been validated using well-known metrics based on the Jacobian. In all our experiments, the β parameter of the t-FFD method [24] has been set to 10 and 2.5 for the inverse and reconstruction process respectively.

4.1. Accuracy and quality evaluation

The proposed method is evaluated using two representative bones of the human foot, namely the first metatarsal and talus (see Figure 6). These bones have been derived through a detail CT scan on a healthy male subject and a reverse

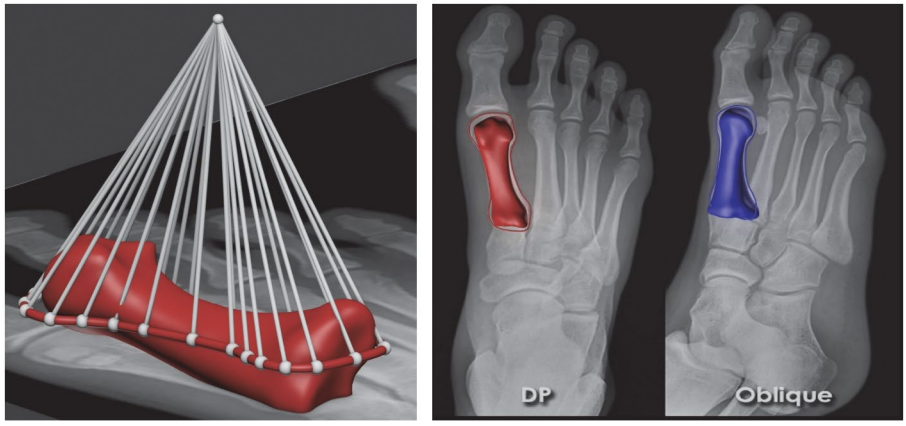

Figure 5. (a) Calibration procedure of the bone with the contour silhouette on the X-ray. (b) Calibration of the bone on the left and right contour.

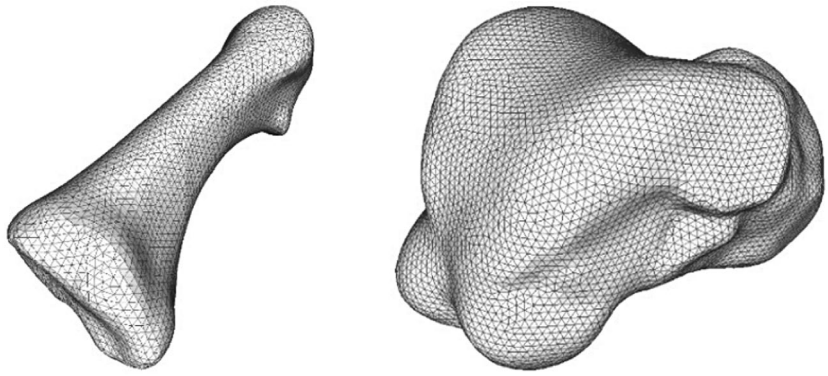

Figure 6. (Left) The metatarsal and (right) talus bones which are used for the accuracy evaluation of the proposed method.

engineering approach based on the screened Poisson surface reconstruction method [33]. Two datasets of bones have been developed by applying linear and non-linear deformations to the original bones of Figure 6. Linear deformations include scaling in X–Y–Z axis while nonlinear deformations include twisting and bending along the longitudinal axis of each bone. Under this way, we are able to evaluate the PBD method using complex parameters that are not based solely on one dimensional measurements, like lengths or perimeters. Thirty-one sample bones have been developed for each data-set, while the number of triangles of the produced bone models varies between 8.600 and 12.000. For the generation of the corresponding parametric models we have used 25 out of the 31 models of each dataset. The rest six have been used for evaluation purposes. In the sequel, the metatarsal test bones are denoted by Mi, while the tarsus test bones by Ti, where $i = 1, \ldots 6$.

Five different parameters have been selected to describe semantically the shape of the bones: Maximum length along the x-axis (L); Maximum width along the y-axis (W); Maximum height along the z-axis (H); Bending along the x-axis (B); Twisting along the x-axis (T).

Figures 7 and 8 portray, using color maps, the difference between the original and the new bone for each of the six bones in our database that haven't be included in the production of the parametric model of the first metatarsal and talus, respectively. In-depth comparisons are given in Tables 1 and 2. The length/width/height values of the reconstructed bones are denoted as L', W' and H', respectively.

In order to examine the accuracy of the produced models four error metrics have been employed, namely: percentage length/width/height difference (%), maximum ($D_{\max}$), mean (D_{mean}) and standard deviation (SD). All distance measurements are in mm.

The percentage difference of L, W, H is quite small (less than 0.5 mm error) in most of the cases for both metatarsal and talus. Bone models M4 and T4 show the highest deviation among all generated bones due to the large amount of distortion that has been applied to the original bones, which also indicates an under-sampling problem. Three-dimensional deviation analysis gives very small differences. Except for M4 all values of $D_{\max}$ are less than 0.5 mm. Similarly, D_{mean} and SD are very

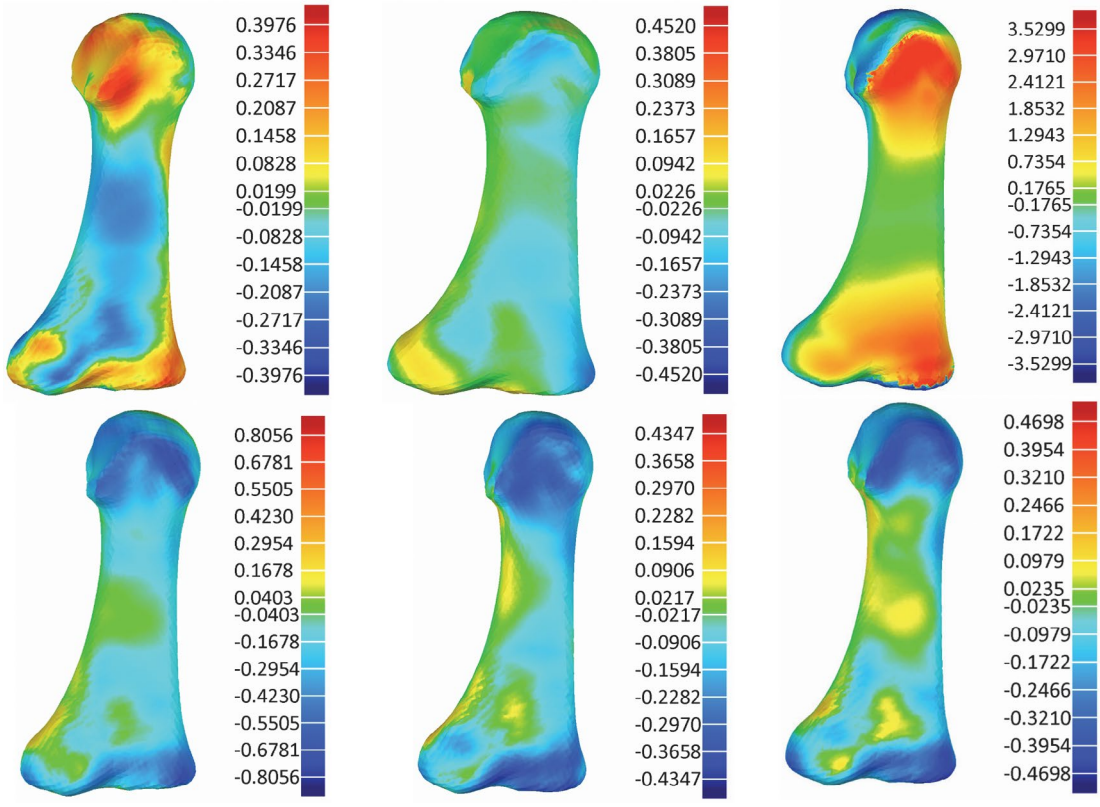

Figure 7. Color maps indicating the differences between the original and generated bones of the first metatarsal (bones M1–M6).

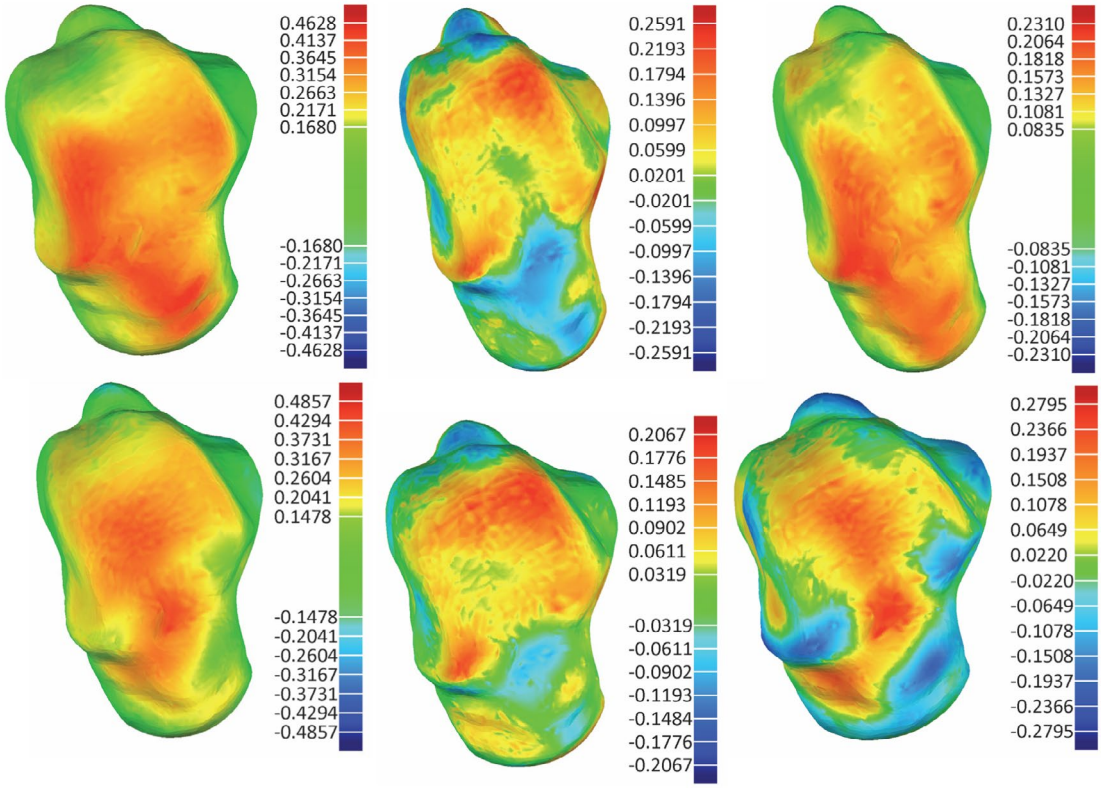

Figure 8. Color maps indicating the differences between the original and generated bones of the talus (bones T1–T6).

Table 1. Deviation analysis of different instances of the first metatarsal bone (mesh models M1–M6) and comparison with [11].

	M1	M2	M3	M4	M5	M6
	$B=-14$	$B=4$	$B=18$	$B=-14$	$B=5$	$B=0$
Param\Model	$T=-12$	$T=-5$	$T=0$	$T=12$	$T=5$	$T=5$
L	68.2091	68.7950	70.5383	85.8114	84.3588	82.7127
L'	68.2277	68.8078	70.7181	85.8988	84.2483	82.5887
Difference %	0.0273%	0.0186%	0.2549%	0.1019%	0.1310%	0.1499%
W	29.5984	35.4369	30.8595	38.6583	36.6585	35.3481
W'	29.9775	35.3651	30.9506	37.9910	36.2958	35.0384
Difference %	1.28%	0.20%	0.30%	1.73%	0.99%	0.88%
H	23.4515	26.4352	23.8311	29.1466	24.7800	29.1835
H'	23.5938	26.0452	23.9452	28.3553	24.4677	28.5144
Difference %	0.61%	1.48%	0.48%	2.71%	1.26%	2.29%
D_{max}	0.3976	−0.452	0.3809	−0.8056	−0.4347	−0.4698
D_{mean}	0.1111	−0.0805	−0.0834	−0.1529	−0.1054	−0.1075
SD	0.1345	0.0808	0.1005	0.1763	0.1059	0.0961
D_{max} using [11]	0.5634	−1.2591	−0.6827	−1.2519	−0.6417	−0.5349
Improvement %	41.70%	178.56%	79.23%	55.40%	47.62%	14.54%
D_{mean} using [11]	0.1363	−0.2222	−0.1381	−0.2289	−0.1405	−0.1123
Improvement %	22.68%	176.02%	65.59%	49.71%	33.30%	4.47%
SD using [11]	0.153	0.2386	0.1377	0.29	0.1366	0.1083
Improvement %	13.75%	195.30%	37.01%	64.49%	28.99%	12.70%

Table 2. Deviation analysis of different instances of the talus bone (mesh models T1-T6) and comparison with [11].

	T1	T2	T3	T4	T5	T6
	$B=-8$	$B=8$	$B=-6$	$B=-9$	$B=9$	$B=-4$
Param\Model	$T=-4$	$T=3$	$T=-4$	$T=5$	$T=6$	$T=4$
L	43.0734	43.0700	43.9994	46.3064	47.6981	54.1815
L'	43.2013	43.1754	44.0633	46.3249	47.6381	53.9318
Difference %	0.30%	0.24%	0.15%	0.04%	0.13%	0.46%
W	36.5225	37.6290	36.5636	43.8873	39.5625	45.8693
W'	37.5866	37.7880	37.1914	44.5837	39.7799	45.9924
Difference %	2.91%	0.42%	1.72%	1.59%	0.55%	0.27%
H	60.8282	77.0992	77.7611	74.5978	72.5100	73.1131
H'	61.1373	77.1340	77.7742	74.6080	72.5837	72.9680
Difference %	0.51%	0.05%	0.02%	0.01%	0.10%	0.20%
D_{max}	0.4628	−0.2591	0.231	0.4857	−0.2067	0.2795
D_{mean}	0.1583	−0.0682	0.0647	0.1243	0.0498	0.0621
SD	0.1187	0.0746	0.0618	0.1071	0.0574	0.0721
D_{max} using [11]	0.6371	0.475	0.4175	1.0342	0.6177	0.493
Improvement %	37.66%	83.33%	80.74%	112.93%	198.84%	76.39%
D_{mean} using [11]	0.2071	0.081	0.1373	0.2331	0.113	0.0912
Improvement %	30.83%	18.77%	112.21%	87.53%	126.91%	46.86%
SD using [11]	0.1586	0.0949	0.1046	0.2237	0.1281	0.1016
Improvement %	33.61%	27.21%	69.26%	108.87%	123.17%	40.92%

Table 3. Histograms of normalized average Condition Number $\mathcal{K}$ of triangles in original first metatarsal mesh (prototype) and the deformed meshes of Table 1.

κ\Model	Proto-type	M1	M2	M3	M4	M5	M6
1.0–1.5	10387	10382	10434	10387	10504	10528	10483
1.5–2.0	620	614	604	616	566	554	602
2.0–3.0	364	373	359	364	346	339	359
3.0–4.0	119	121	110	125	101	93	125
4.0–5.0	53	51	43	54	49	53	55
5.0–7.5	88	86	91	88	80	82	81
7.5–10.0	43	46	40	40	35	33	40
10.0–15.0	42	40	35	45	38	39	41
15.0–20.0	12	15	12	11	9	7	12

low in all generated bones, implying that both linear and nonlinear deformations have been regenerated accurately.

We have also evaluated the quality of the triangulations of the deformed meshes Mi and Ti, using the condition number of the Jacobian of each mesh triangle which represents a measure of its shape; the closer to one the better the shape of the triangle is [34]. We have normalized the condition numbers of the triangles in the range $[1, 20]$ and created the histograms shown in Tables 3 and 4. It can be observed that the quality of the triangulation of the deformed meshes remains almost the same to the quality of the triangulation of the prototype mesh. Additionally, all the produced meshes in this paper have been checked for quality issues, like foldovers, spikes, non-manifold edges, self-intersections, etc., using commercial software and no defects have been found. This shows that the proposed PBD method (and the underlying FFD algorithm)

Table 4. Histograms of normalized average condition number $\mathcal{K}$ of triangles in original talus mesh (prototype) and the deformed meshes of Table 2.

$\mathcal{K}$\ Model	Proto-type	T1	T2	T3	T4	T5	T6
1.0–1.5	4728	4698	4431	4593	4683	4686	4722
1.5–2.0	1909	1921	2054	2023	1956	1988	1894
2.0–3.0	1645	1642	1733	1661	1643	1627	1654
3.0–4.0	478	487	506	482	468	461	486
4.0–5.0	187	192	195	178	182	182	188
5.0–7.5	113	123	138	129	135	122	118
7.5–10.0	37	34	42	36	33	35	37
10.0–15.0	16	16	13	12	12	11	14
15.0–20.0	7	7	8	6	8	8	7

does not introduce quality defects in the produced triangle meshes.

4.2. Comparison against the previous approach

In order to establish a common basis for comparison, the set of 3D animal-bone models used in [20] has been acquired. This data-set consists of 13 right metatarsal bone models of chicken legs. Similarly, we use bone #7 as a template model and reproduce all thirteen bones using five parameters according to the parameter set 5(b) reported in [20].

Table 5 lists the results of the reconstruction of all 13 chicken metatarsal bones using absolute values for $D_{\max}$ and SD. The proposed method produced bone meshes which according to $D_{\max}$ are improved compared to [20] in the range 21.83–43.66%. Only bone models #3 and #7 have larger deviation error compared to the original method. The mean error deviation with the new method is 1.12 mm while with the previous one is 1.57 mm, implying a 28.66% improvement.

4.3. Comparison against a PCA-based method

The proposed method has been compared against PCA-based methods like [4] and [11] and all experimental results indicate a significant improvement of the accuracy of the generated bone models. Works [4] and [11] are similar in spirit, and therefore, we chose to present the comparison results with [11], which emphasizes on the use of semantic parameters. Tables 1 and 2 depict a direct comparison with the work reported in [11]. In all cases, the proposed method provides superior results with respect to the three accuracy indices $D_{\max}$, D_{mean}, and SD.

For the first metatarsal, $D_{\max}$ improvement is between 14.54 and 178.56%, D_{mean} between 4.47 and 176.02%, and SD between 12.70 and 195.30%. Similar results are derived for the talus bone where $D_{\max}$ improvement is between 37.66 and 198.84%, D_{mean} between 18.77 and 126.91%, and SD between 27.21 and 123.17%.

For the generation of models using the PCA-based method, a large 95% ratio of principal components has been used, while the simplified control mesh used in our approach consists of merely 37 vertices. Figure 9, illustrates the comparison results for the metatarsal bone.

5. Evaluation of the method for the reconstruction of a bone from its bi-planar X-ray: application in bioengineering analysis

Algorithm A, presented in Section 3, is applied for the parametric reconstruction of custom foot bones and the results are evaluated. For clarity reasons, the reconstruction and evaluation are performed using the first metatarsal bone.

Figure 10, illustrates the 7 semantic parameters chosen to create the corresponding parametric model. Their measurements are computed automatically using the silhouette contour S_i as described in Step A.3 of Algorithm A.

The principal direction of each bone is found from its contour points using PCA. Parameter No#1, represents the length d of the line segment generated from the intersection of the principal axis with the silhouette contour (Figure 10). The rest of the transversal measurements are calculated by shooting perpendicular rays at the silhouette principal axis at points m, $m \pm 3d/8$, where m is the center of mass of each silhouette. These measurements correspond to the parameters No#2 – No#7 of Figure 10.

5.1. Evaluation

The proposed algorithm has been evaluated using a new biplanar X-ray of a male subject along with the corresponding CT scan (Figure 11), and the chicken metatarsal data-set [20]. In addition, a parametric analysis has been carried out to investigate the sensitivity of the proposed application to the number of semantic parameters.

Figure 12, shows a new X-ray with the two contours of the first metatarsal highlighted. The parametric model of this bone has been developed using the seven semantic

Table 5. Deviation analysis of thirteen chicken metatarsal bones and comparison with [20].

Error\Model	1	2	3	4	5	6	7	8	9	10	11	12	13
$D_{\max}$	1.11	1.11	1.60	1.22	0.9	1.02	0.8	1.33	0.97	1.2	1.13	1.13	1.06
$D_{\max}$ in [20]	1.77	1.42	1.31	2.03	1.25	1.72	0.69	1.33	1.49	2.13	1.81	1.87	1.56

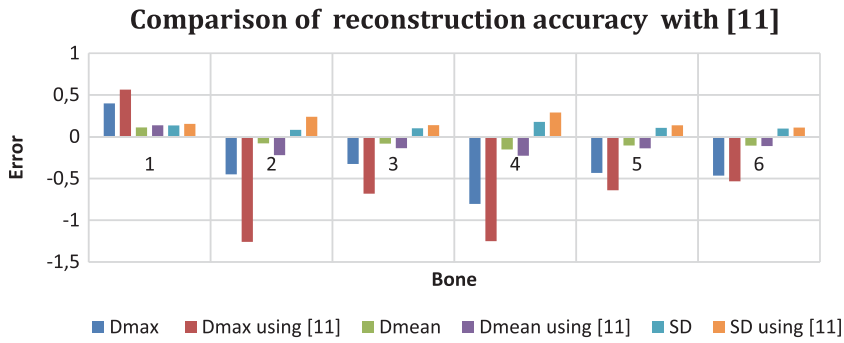

Figure 9. Comparison of reconstruction accuracy with [11] for the 1st metatarsal.

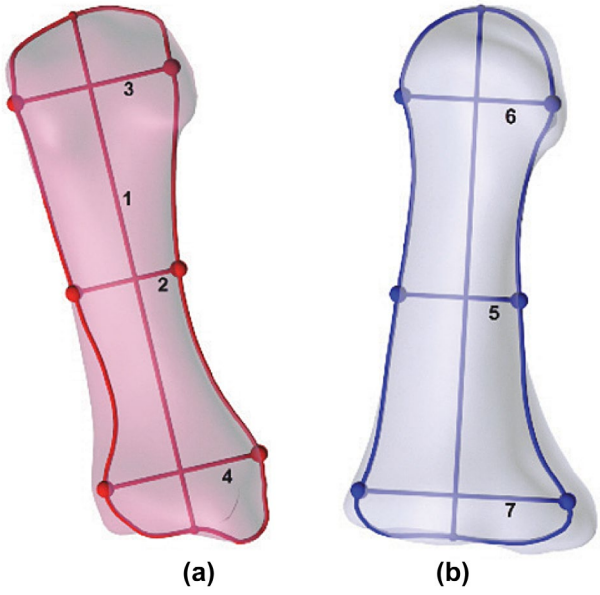

Figure 10. The seven semantic parameters of the 1st metatarsal bone.

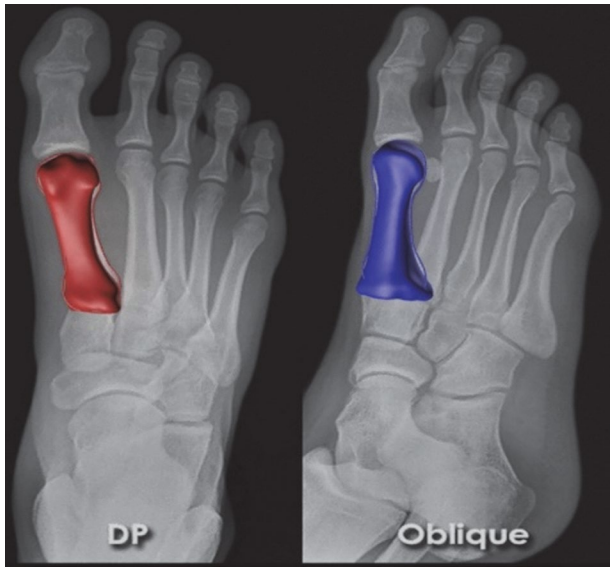

Figure 11. Reconstruction of the first metatarsal bone according to the measurements taken on the biplanar X-ray.

parameters explained above. The final model has been compared with the real CT-scanned bone of the same subject as it is shown in Figure 13, where the corresponding 3D deviation analysis is given. The error metrics show an accurate reconstruction: D_{max} = 2.38 mm, D_{mean} = –0.58 mm and SD = 0.70 mm.

A second evaluation of the proposed algorithm is performed using the animal metatarsal bones. Since these constitute a data-set of real bones, where their corresponding 3D mesh model is available through 3D scanning, the comparison of the produced instances against the original ones is straightforward. The detailed results of the corresponding deviation analysis are given in Table 6 and depict an accurate reconstruction.

In all samples, the maximum errors occur in areas of high curvature (e.g. sharp corners or occluded regions) and are also related to scanning difficulties in these areas. For the purposes of reconstructing a foot biomodel for mechanical analysis, this level of error is considered acceptable since the corresponding FE model of each bone is subject to smoothing and simplification during the pre-processing stage. Therefore, errors that occur mainly in sharp regions will be abbreviated by the FE pre-processor.

5.2. Parameter sensitivity analysis

The number and nature of the selected semantic parameters is subject to the specific application and geometry of the corresponding data-set. The semantic parameters must be selected by the help of a specialist like a radiologist. To all our knowledge this is a standard procedure followed by all similar applications. Having only one or two parameters is likely to be poor, whereas having a large set of parameters could render the entire reconstruction approach impractical. We test the robustness of the proposed algorithm using four different variations of parameters shown in Figure 10 to reconstruct the chicken metatarsal bones, as follows:

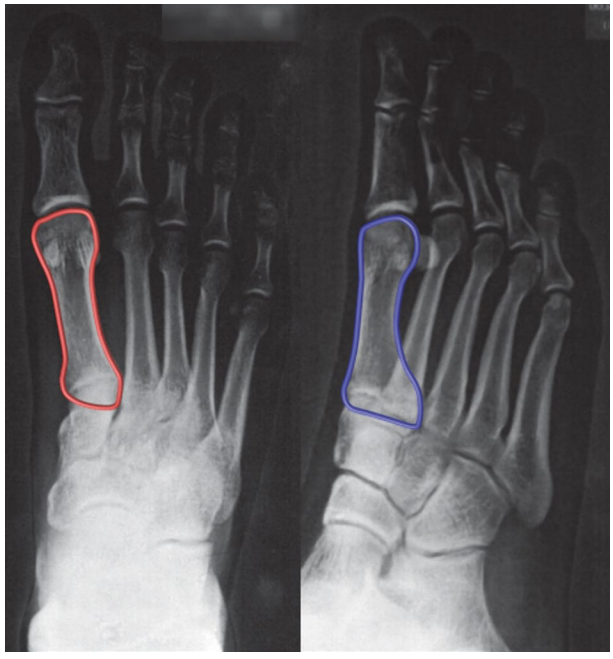

Figure 12. A new biplanar X-ray with the two contours of the first metatarsal highlighted.

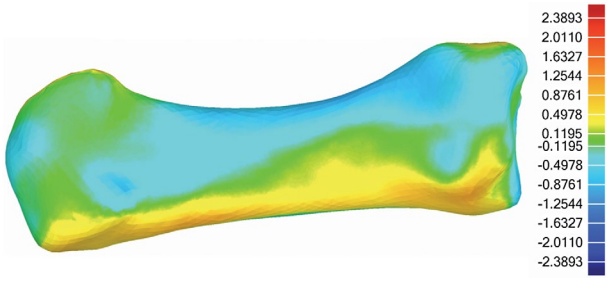

Figure 13. The 3D deviation analysis of the derived bone against the real one derived through CT scan.

Table 6. The error metrics depicting the deviation of the produced animal bones against the real ones.

Error/Model	2	7	10	13	3	5	9
D_{max}	2.64	1.71	1.04	−1.47	3.34	2.26	3.03
D_{mean}	0.28	0.12	0.25	0.3	0.61	0.53	0.69
SD	0.38	0.19	0.29	0.32	0.79	0.61	0.82

- 3 parameters: they correspond to parameters 1, 2, 5.
- 5 parameters: they correspond to parameters 1, 2, 5, 3, 7.
- 7 parameters: they correspond to parameters 1, 2, 3, 4, 5, 6, 7.
- 9 parameters: they correspond to parameters 1, 2, 3, 4, 5, 6, 7, 8, 9, where the new parameters 8 & 9 correspond to transversal widths in the DP and in the Oblique view respectively.

Figures 14–16 illustrate the three error-metrics D_{max}, D_{mean}, and SD (we use their absolute value for simplicity of presentation). All results are given in mm. According to D_{max}, there is a significant improvement up to 49% with the use of 7 or 9 parameters instead of 3 or 5. Although in general the more parameters used, the less the error is, bone #12 seems to be an exception. Also, bone #13 seems that is not getting any improvement with the increase in the parameters. However, metric D_{mean} at Figure 15 and metric SD at Figure 16 clearly indicate a significant improvement of bone #12 (about 24%) and a fair improvement of bone #13 when 9 parameters are used. A more detailed examination of the D_{max} results, shows that these errors are located in sharp regions of the bone and may indicate under-sampling problems.

Several experiments have been conducted for the determination of the number of control vertices of the simplified control mesh. We have set the number of control vertices between 20 and 60, and then test the accuracy of the respective parametric model. For the current skeletal models, we noticed no improvement with more than 37 vertices in the control mesh. Therefore, all the experiments presented in this paper utilize this number of control vertices.

5.3. Application of the produced biomodel in bioengineering analysis

Using the proposed algorithm, we were able to produce a parametric biomodel of the human foot and reproduce all the metatarsal bones according to the custom foot depicted in the biplanar X-ray (Figure 4). We have used a

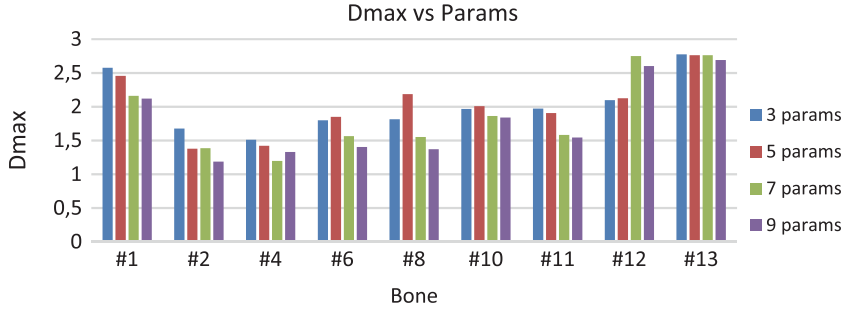

Figure 14. The deviation analysis of the derived chicken metatarsal bones according to the absolute D_{max} metric.

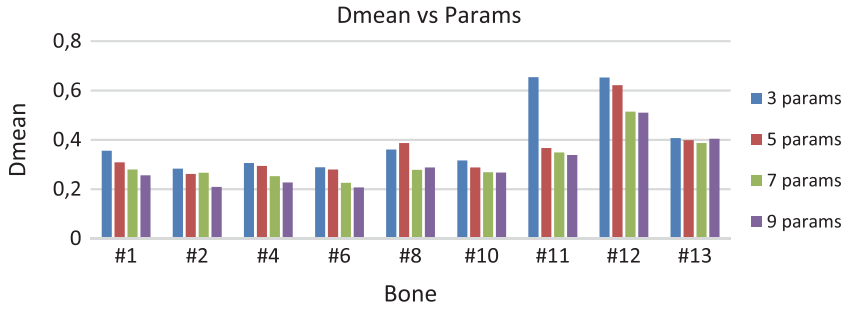

Figure 15. The deviation analysis of the derived chicken metatarsal bones according to the absolute D_{mean} metric.

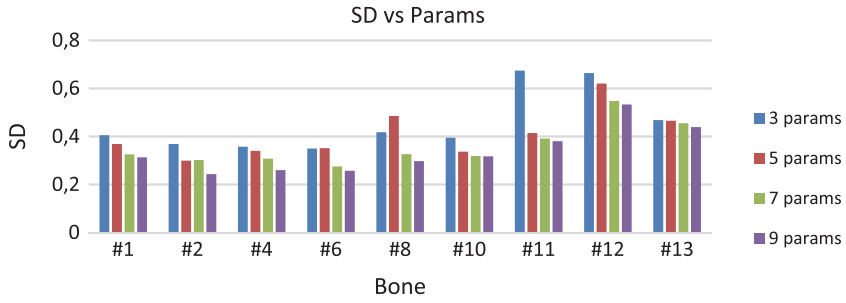

Figure 16. The deviation analysis of the derived chicken metatarsal bones according to the absolute SD metric.

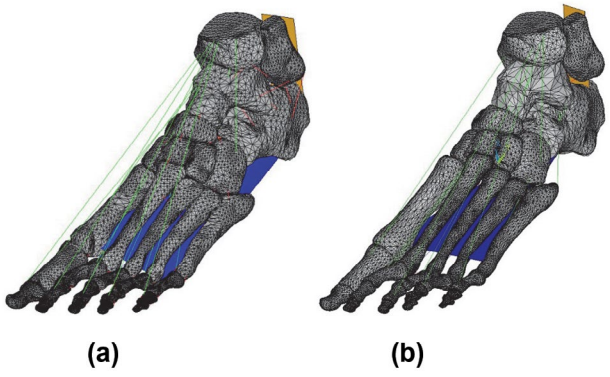

Figure 17. (a) The template biomodel and (b) the new custom biomodel of the proposed approach.

template biomodel developed using CT scans of a healthy person. The template biomodel consists of 26 bone meshes (plus 2 bone parts of Tibia and Fibula), 33 joints and various tendons.

Using the template biomodel, a new (custom) biomodel has been derived as shown in Figure 17. The metatarsal bones of the new biomodel comply with the measurements of the metatarsal bones in the X-ray. The new biomodel can be applied for bioengineering analysis using the FEM.

6. Conclusions

In this paper, two methodologies related to human bone reconstruction have been proposed. Based on the work reported in [20], a revised reconstruction method for 3D skeletal models has been introduced that overcomes limitations of the original approach and is able to provide superior reconstruction accuracy compared to statistical-based methods. The new method can handle detailed and dense models with thousands of triangle elements and has been applied successfully to different data-sets of human and animal bone models.

A new algorithm has been described for the generation of parametric bone models of the human foot using non-calibrated biplanar X-rays. The proposed method is using a 3D template biomodel of the human foot to produce new instances of foot biomodels based on biplanar X-rays. This method has been evaluated with both human and animal bones.

All produced bone models have been tested for quality issues using metrics based on the Jacobian [34] and for geometric defects like foldovers, spikes, non-manifold edges, self-intersections, and found zero defects. This implies that the produced meshes can be used for analysis applications. The current geometric-based approach seems promising compared to well-established statistical approaches based on PCA.

The research results presented in the paper have been implemented in a cloud-based application for automating the development of parametric foot bone models and for the production of custom foot biomodels. The application can be found by following this link: http://optshoes.azurewebsites.net/

Future research efforts will be focused on developing a fully automated procedure for producing foot biomodels.

Acknowledgments

This research has been co-financed by the European Social Fund and national funds through the Operational Program Education and Lifelong Learning of the National Strategic Reference Framework (NSRF) – Research Funding Program 'ARISTEIA.' The authors wish to thank Prof. Ajay Joneja of Hong Kong University, for providing the dataset of animal bones.

Disclosure statement

No potential conflict of interest was reported by the authors.

Notes on contributors

Alexander Agathos is a researcher at the Department of Product and Systems Design Engineering of the University of The Aegean. His research interests span the areas of Computer Graphics, Computer Vision, Hyperspectral Imaging and Machine Learning.

Philip Azariadis, PhD, is a professor with the Department of Product & Systems Design Engineering at the University of the Aegean. His research activities are focused in the areas of Product Design (Computer-Aided Design, 3D Modelling for engineers), Reverse Engineering, Motion Design, Routing/Scheduling and Computer Graphics. His research work has found industrial applications in the footwear, garment and jewellery industries, and has been published in leading scientific journals and conferences. He has been involved as a researcher or scientific coordinator in numerous European or National R&D projects and served as a reviewer in 35 international journals and in several international and national founding organisations. He has been reviewer and member of the international programme committee of more than 100 international conferences, while he is member of the editorial board of 3 international journals.

ORCID

Alexander Agathos http://orcid.org/0000-0002-0402-0821
Philip Azariadis http://orcid.org/0000-0002-8687-5777

References

[1] Azariadis P. Finite element analysis in footwear design. In: Goonetilleke R., editor. The science of footwear. Taylor & Francis Group; 2012. p. 321–337.
[2] Baka N, Kaptein B, de Bruijne M, et al. 2D–3D shape reconstruction of the distal femur from stereo X-ray imaging using statistical shape models. Med Image Anal. 2011;15(6):840–850.
[3] Zheng G, Gollmer S, Schumann S, et al. A 2D/3D correspondence building method for reconstruction of a patient-specific 3D bone surface model using point distribution models and calibrated X-ray images. Med Image Anal. 2009;13(6):883–899.
[4] Allen B, Curless B, Popović Z. The space of human body shapes: reconstruction and parameterization from range scans. ACM Trans Graph. 2003;22(3):587–594.
[5] Hasler N, Stoll C, Sunkel M, et al. A statistical model of human pose and body shape. Comp Graph Forum. 2009;28(2):337–346.
[6] Kwok T-H, Yeung K-Y, Wang CC. Volumetric template fitting for human body reconstruction from incomplete data. J Manuf Syst. 2014;33(4):678–689.
[7] Seo H, Magnenat-Thalmann N. An automatic modeling of human bodies from sizing parameters. In: Proceedings of the 2003 Symposium on Interactive 3D Graphics. New York (NY): ACM; 2003. p. 19–26.
[8] Seo H, Cordier F, Magnenat-Thalmann N. Synthesizing animatable body models with parameterized shape modifications. In: Proceedings of the 2003 ACM SIGGRAPH/Eurographics Symposium on Computer Animation, SCA '03; Aire-la-Ville, Switzerland: Eurographics Association; 2003. p. 120–125.
[9] Wang CC, Wang Y, Chang TK, et al. Virtual human modeling from photographs for garment industry. Comput Aided Des. 2003;35(6):577–589.
[10] Wang CC. Parameterization and parametric design of mannequins. Comput Aided Des. 2005;37(1):83–98.
[11] Chu C-H, Tsai Y-T, Wang CCL, et al. Exemplar-based statistical model for semantic parametric design of human body. Comput Ind. 2010;61(6):541–549.
[12] Fleute M, Lavallée S, Julliard R. Incorporating a statistically based shape model into a system for computer-assisted anterior cruciate ligament surgery. Med Image Anal. 1999;3(3):209–222.
[13] Cootes T, Taylor C, Cooper D, et al. Active shape models-their training and application. Comput Vision Image Understanding. 1995;61(1):38–59.
[14] Le Bras A, Laporte S, Bousson V, et al. 3D reconstruction of the proximal femur with low-dose digital stereoradiography. Comput Aided Surgery. 2004;9(3):51–57.
[15] Humbert L, Guise JD, Aubert B, et al. 3D reconstruction of the spine from biplanar X-rays using parametric models based on transversal and longitudinal inferences. Med Eng Phys. 2009;31(6):681–687.
[16] Pomero V, Mitton D, Laporte S, et al. Fast accurate stereoradiographic 3D-reconstruction of the spine using a combined geometric and statistic model. Clin Biomech. 2004;19(3):240–247.
[17] Luximon A, Goonetilleke RS. Foot shape modeling. Human Factors. 2004;46(2):304–315.
[18] Luximon A, Goonetilleke RS, Zhang M. 3D foot shape generation from 2D information. Ergonomics. 2005;48(6):625–641.
[19] Tang Y-M, Hui K-C. Human foot modeling towards footwear design. Comput Aided Des. 2011;43(12):1841–1848.
[20] Lee J, Joneja A. A study on parametric shape modifications of 3D skeletal models. Comput Aided Des Appl. 2014;11(1):90–98.
[21] Agathos A, Azariadis P. Parametric-based reconstruction Of 3D mesh models; Towards the generation of a parametric human foot biomodel. Eurographics Workshop on Visual Computing for Biology and Medicine; 2015.
[22] Baudoin A, Skalli W, de Guise J, et al. Parametric subject-specific model for *in vivo* 3D reconstruction using bi-planar X-rays: application to the upper femoral extremity. Med Biol Eng Comput. 2008;46(8):799–805.

[23] Garland M, Heckbert PS. Surface simplification using quadric error metrics. In: Proceedings of the 24th Annual Conference on Computer Graphics and Interactive Techniques, SIGGRAPH '97. Los Angeles, CA; 1997. p. 209–216.
[24] Kobayashi KG, Ootsubo K. t-ffd: free-form deformation by using triangular mesh. In: Proceedings of the Symposium on Solid Modeling and Applications; 2003. p. 226–234.
[25] Feldmar J, Ayache N. Rigid, affine and locally affine registration of free-form surfaces. Int J Comput Vision. 1996;18(2):99–119.
[26] Marquardt DW. An algorithm for least-squares estimation of nonlinear parameters. SIAM J Appl Math. 1963;11(2):431–441.
[27] Campbell S, Meyer C. Generalized inverses of linear transformations, classics in applied mathematics. SIAM; 2009.
[28] Cheung TM, Zhang M, Leung KL, et al. Three-dimensional finite element analysis of the foot during standing, a material sensitivity study. J Biomech. 2005;38(5):1045–1054.
[29] Lewis G. Finite element analysis of a model of a therapeutic shoe: effect of material selection for the outsole. Biomed Mater Eng. 2003;13(1):75–81.
[30] Chen WP, Ju CW, Tang F. Effects of total contact insoles on the plantar stress redistribution: a finite element analysis, Clin Biomech. 2003;18(6):17–24.
[31] Koutkalaki Z, Papagiannis P, Azariadis P, et al. Towards a foot bio-model for performing finite element analysis for footwear design optimization using a cloud infrastructure. Comput Aided Design Appl. 2015; 12:507–518.
[32] Lavallee S, Szeliski R. Recovering the position and orientation of free-form objects from image contours using 3D distance maps. IEEE Trans Pattern Anal Mach Intell. 1995;17(4):378–390.
[33] Kazhdan M, Hoppe H. Screened Poisson surface reconstruction. ACM Trans Graph. New York 2013;32(3):1–29:13.
[34] Garimella RV, Shashkov MJ, Knupp PM. Triangular and quadrilateral surface mesh quality optimization using local parametrization. Comput Meth Appl Mech Eng. 2004;193(911):913–928.